Fusion of Low-Cost Imaging and Inertial Sensors for Navigation

Major M. Veth, *Air Force Institute of Technology*
J. Raquet, *Air Force Institute of Technology*

BIOGRAPHY

Major Mike Veth is a Ph.D. student in the Department of Electrical and Computer Engineering at the Air Force Institute of Technology. His current research focus is on the fusion of imaging and inertial systems for navigation. He received his M.S. in Electrical Engineering from the Air Force Institute of Technology, and a B.S. in Electrical Engineering from Purdue University. In addition, Major Veth is a graduate of the Air Force Test Pilot School.

John Raquet is an associate professor in the Department of Electrical and Computer Engineering at the Air Force Institute of Technology, where he is also the Director of the Advanced Navigation Technology Center. He has been involved in navigation-related research for over 15 years.

ABSTRACT

Aircraft navigation information (position, velocity, and attitude) can be determined using optical measurements from imaging sensors combined with an inertial navigation system. This can be accomplished by tracking the locations of optical features in multiple images and using the resulting geometry to estimate and remove inertial errors.

A critical factor governing the performance of image-aided inertial navigation systems is the robustness of the feature tracking algorithm. Previous research has shown the strength of rigorously coupling the image and inertial sensors at the measurement level using a tactical-grade inertial sensor. While the tactical-grade inertial sensor is a reasonable choice for larger platforms, the greater physical size and cost of the sensor limits its use in smaller, low-cost platforms.

In this paper, an image-aided inertial navigation algorithm is implemented using a multi-dimensional stochastic feature tracker. In contrast to previous research, the algorithms are specifically evaluated for operation using low-cost, CMOS imagers and MEMS inertial sensors. The performance of the resulting image-aided inertial navigation system is evaluated using Monte Carlo simulation and experimental data and compared to the performance using more expensive inertial sensors.

INTRODUCTION

Motivation

As mentioned in our previous research [18], [24], [22], the benefits of tightly integrating navigation sensors, such as inertial measurement units (IMU) and global positioning system (GPS) receivers, is well-known. The complimentary characteristics of the two sensors allow the integrated system to perform at levels which are difficult to attain with either sensor alone (see [3]). As a result, integrated IMU/GPS systems have become common, especially in military-grade navigation systems. Unfortunately, GPS signals are not available in all locations, which motivates the development of a non-GPS based navigation reference which can aid an inertial navigation system.

One non-GPS navigation approach is to integrate a camera with an inertial sensor [19], [17], [2]. This technique has some important advantages. Foremost, the sensors can operate in environments where GPS is difficult to receive (e.g., indoors, under trees, underwater, etc.). Secondly, the sensors are completely passive and do not require the transmission (or reception) of radio signals. As a result, optical and inertial sensors are immune to disruptions in the radio spectrum.

Previous work has shown the value of fusing images and inertial measurements for navigation [23]. In this paper, an image-aided inertial navigation algorithm is implemented using a multi-dimensional stochastic feature tracker. In contrast to previous research, the algorithms are specifically evaluated for operation on low-cost, complementary metal-oxide semiconductor (CMOS) imagers and micro-electro-mechanical systems (MEMS) consumer-grade inertial sensors. The performance of the resulting image aided inertial navigation system is evaluated using Monte Carlo simulation and experimental data and compared to the performance using tactical-grade inertial sensors. This effort

Report Documentation Page

Form Approved
OMB No. 0704-0188

1. REPORT DATE	2. REPORT TYPE	3. DATES COVERED
2007		**00-00-2007 to 00-00-2007**

4. TITLE AND SUBTITLE	5a. CONTRACT NUMBER
Fusion of Low-Cost Imaging and Inertial Sensors for Navigation	5b. GRANT NUMBER
	5c. PROGRAM ELEMENT NUMBER
6. AUTHOR(S)	5d. PROJECT NUMBER
	5e. TASK NUMBER
	5f. WORK UNIT NUMBER
7. PERFORMING ORGANIZATION NAME(S) AND ADDRESS(ES) **Air Force Institute of Technology,2950 Hobson Way,Wright Patterson AFB,OH,45433-7765**	8. PERFORMING ORGANIZATION REPORT NUMBER
9. SPONSORING/MONITORING AGENCY NAME(S) AND ADDRESS(ES)	10. SPONSOR/MONITOR'S ACRONYM(S)
	11. SPONSOR/MONITOR'S REPORT NUMBER(S)

12. DISTRIBUTION/AVAILABILITY STATEMENT
Approved for public release; distribution unlimited

13. SUPPLEMENTARY NOTES
The original document contains color images.

14. ABSTRACT

15. SUBJECT TERMS

16. SECURITY CLASSIFICATION OF:			17. LIMITATION OF ABSTRACT	18. NUMBER OF PAGES	19a. NAME OF RESPONSIBLE PERSON
a. REPORT	b. ABSTRACT	c. THIS PAGE			
unclassified	**unclassified**	**unclassified**		**11**	

is part of ongoing research into fusion of imaging and inertial sensors for long-term autonomous navigation.

Current Methods

It is well-known that optical measurements provide excellent navigation information, when interpreted properly. Optical navigation is not new. Pilotage is the oldest and most natively familiar form of navigation to humans and other animals. For centuries, navigators have utilized mechanical instruments such as astrolabes, sextants, and driftmeters [14] to make precision observations of the sky and ground in order to determine their position, velocity, and attitude.

The difficulty in using optical measurements for autonomous navigation (that is, without human intervention) has always been in the interpretation of the image, a difficulty shared with Automatic Target Recognition (ATR). Indeed, when celestial observations are used, the ATR problem in this structured environment is tractable, and automatic star trackers are widely used for space navigation and ICBM guidance [6, 15, 16]. When ground images are to be used, the difficulties associated with image interpretation are paramount. At the same time, the problems associated with the use of optical measurements for navigation are somewhat simpler than ATR. Moreover, recent developments in feature tracking algorithms, miniaturization, and reduction in cost of inertial sensors and optical imagers, aided by the continuing improvement in microprocessor technology, motivates the use of inertial measurements to aid the task of feature tracking in image sequences.

Image-aiding methods are typically classified as either feature-based or optic flow-based, depending on how the image correspondence problem is addressed. Feature-based methods determine correspondence for "landmarks" in the scene over multiple frames, while optic flow-based methods typically determine correspondence for a whole portion of the image between frames. A good reference on image correspondence is [8]. Optic flow methods have been proposed generally for elementary motion detection, focusing on determining relative velocity, angular rates, or obstacle avoidance [5].

Feature tracking-based navigation methods have been proposed both for fixed-mount imaging sensors or gimbal mounted detectors which "stare" at the target of interest, in a manner similar to the gimballed infrared seeker on heat-seeking, air-to-air missiles. Many feature tracking-based navigation methods exploit knowledge (either *a priori*, through binocular stereopsis, or by exploiting terrain homography) of the target location and solve the inverse trajectory projection problem [1, 12]. If no *a priori* knowledge of the scene is provided, egomotion estimation is completely correlated with estimating the scene. This is referred as the structure from motion (SFM) problem. A theoretical development of the geometry of fixed-target tracking, with no *a priori* knowledge is provided in [13]. An online (Extended Kalman Filter-based) method for calculating a trajectory by tracking features at an unknown location on the Earth's surface, provided the topography is known is given in [4]. Finally, navigation-grade inertial sensors and terrain images collected on a T-38 "Talon" were processed and the potential benefits of optical-aided inertial sensors are experimentally demonstrated in [17].

A rigorous, stochastic projection algorithm is presented in [24], which incorporates inertial measurements into a predictive feature transformation, effectively constraining the resulting correspondence search space. The algorithm was incorporated into an extended Kalman filter and tested experimentally in [23] using a tactical-grade inertial sensor. The integrated system demonstrated at least two orders of magnitude improvement over the inertial-only navigation solution.

In this paper, the method of stochastic projections [24] is used as the basis for tightly integrating a low-cost MEMS inertial and CMOS imaging sensor using an Extended Kalman Filter (EKF). In the following section, the integration architecture is presented, which includes the underlying assumptions, the inertial mechanization algorithms, EKF state model, measurement model, and feature tracking concept.

DEVELOPMENT

The method proposed in this paper employs an extended Kalman filter (EKF) algorithm [9, 10] to recursively estimate the navigation state and associated errors by tracking the pixel locations of stationary objects in an image-aided inertial system.

Assumptions

This method is based on the following assumptions.

- A strapdown inertial measurement unit (IMU) is rigidly attached to one or more cameras. Synchronized raw measurements are available from both sensors.
- The camera images areas in the environment which contain some stationary objects.
- Binocular measurements are available which provide an indication of range to objects in the environment.
- The inertial and optical sensors' relative position and orientation is known (see [22] for a discussion of boresight calibration procedures).

Algorithm Description

The system parameters (see Table 1) consist of the navigation parameters (position, velocity, and attitude), inertial sensor biases, and a vector describing the location of landmarks of interest ($\mathbf{y}$). The navigation parameters are calculated using body-frame velocity increment ($\Delta\mathbf{v}^b$) and angular increment ($\Delta\boldsymbol{\theta}^b_{ib}$) measurements from the inertial navigation sensor which have been corrected for bias errors using the current filter-computed bias estimates. These measurements are integrated from an initial state in the navigation (local-level) frame using mechanization algorithms described in [21].

Table 1: *System Parameter Definition*

Parameter	Description
$\mathbf{p}^n$	Vehicle position in navigation frame (northing, easting, and down)
$\mathbf{v}^n$	Vehicle velocity in navigation frame (north, east, down)
$\mathbf{C}^n_b$	Vehicle body to navigation frame DCM
$\mathbf{a}^b$	Acclerometer bias vector
$\mathbf{b}^b$	Gyroscope bias vector
$\mathbf{t}^n_m$	Location of landmark m in the navigation frame (one for each landmark currently tracked)
$\mathbf{d}^b$	Camera-to-IMU lever arm in body frame
$\mathbf{C}^b_c$	Camera-to-IMU orientation DCM

An Extended Kalman Filter is constructed to estimate the errors in the calculated system parameters. In order to minimize the effects of linearization errors, the system parameters are periodically corrected by removing the current error estimate [9]. A block diagram of the system is shown in Figure 1.

The position, velocity, and attitude errors were modeled as a stochastic process based on the well-known Pinson navigation error model [21]. The accelerometer and gyroscopic bias errors were each modeled as a first-order Gauss-Markov process [9], based on the specification for the inertial measurement unit (IMU). The landmarks are modeled as stationary with respect to the Earth. A small amount of process noise is added to the state dynamics to promote filter stability [10].

Landmark Track Maintenance

In a practical system, the number of Kalman Filter states is limited by available computer resources. As a result, the number of landmarks actively tracked must be constrained. This inherent limitation motivates the implementation of a track maintenance algorithm.

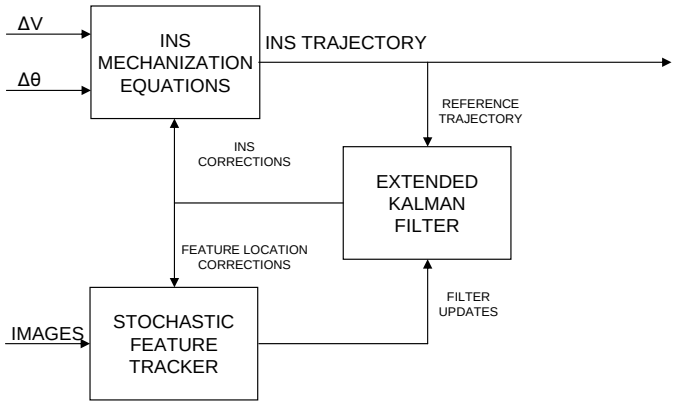

Figure 1: *Image-aided inertial navigation filter block diagram. In this filter, the location of stationary objects are tracked and used to estimate and update the errors in an inertial navigation system. The inertial navigation system is, in turn, used to support the feature tracking loop.*

The general concept for the track maintenance algorithm is to add and prune landmark tracks in order to provide the "best" navigation information to the filter. Although the optimal landmark choices are highly dependent on the trajectory and scene, some general guidelines were used in the track maintenance algorithm.

In general, features which can be easily and accurately tracked for long periods of time provide the best navigation information. This implies choosing features which are: strong and easily identified (to help maintain track), locally distinct (to eliminate false correspondence), and well-separated in image space (to maximize filter observability). Thus, when Kalman Filter landmark track states are available, the feature space of the current image is searched and new landmarks are added based on the above criteria. The filter states are augmented in accordance with the stochastic projection algorithm defined in [24].

In order to maintain only the best tracks, stale landmark tracks (i.e., no successful correspondence available for a given period of time) are pruned by removing the associated filter states. Other track maintenance approaches are possible which could theoretically improve the track performance (e.g., semi-causal, multiple model, or velocity prediction), however these approaches will not be pursued in this paper.

Measurement Model

In order to exploit the synergistic properties of optical and inertial sensors, the navigation and feature tracking algorithms are tightly-coupled. This results in a slight modification to the standard Kalman filter update and propagation cycles in order to incorporate the feature tracking

loop. The tracking loop is responsible for: incorporating new landmark tracks, using stochastic projections to predict and match features between images, providing filter measurements, and deleting stale landmarks from the filter.

The Kalman filter assists the tracking algorithm by maintaining and propagating the minimum mean-square error state estimate. This provides the stochastic projections which help improve the speed and robustness of the tracking loop.

The tracking loop incorporates new landmark tracks when necessary by determining an initial estimate of the landmark location (using either a terrain model or binocular stereopsis combined with the current navigation state vector). This estimate, along with the calculated covariance and cross-correlation matrices are augmented into the Kalman filter state vector and covariance matrix. Details on the mathematics involved in the calculation of the above process are based on the stochastic projection model described in [24].

After the landmark tracks are properly augmented into the Kalman filter, the standard propagation algorithms are used to predict the augmented state to the time of the next image. The location of each landmark (along with arbitrary uncertainty ellipsoid) can then be projected into the feature space of the new image. In this paper, the feature space corresponds to a two-dimensional pixel location and associated uncertainty ellipse. The tracking algorithm then searches this uncertainty ellipse for a feature which has similar characteristics to the reference feature and is distinct. In this paper, a $2-\sigma$ ellipse was used. An example of feature prediction is shown in Figure 2. The reader is referred to [24] for more details regarding the feature prediction algorithm.

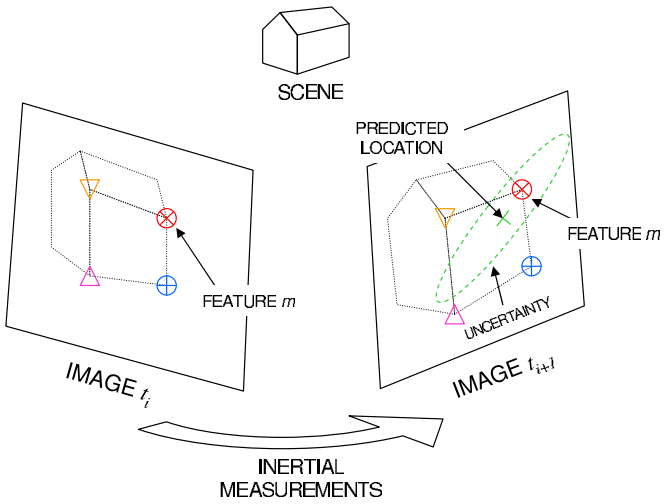

Figure 2: *Stochastic feature projection. Optical features of interest are projected into future images using inertial measurements and stochastic projections.*

Once the landmark tracker has determined a corresponding match, the pixel location of the feature, corrected for optical distortion, is used to update the navigation state. The associated measurement equations are described in further detail in [23].

Measurement Accuracy Considerations

The inertial-aided feature correspondence algorithm presented in the previous section leverages inertial measurements to statistically constrain the feature correspondence search between images. As shown in [24], the correspondence search region is the projection of a random vector into the feature space. The statistics of this random vector are influenced by the inertial measurement errors, the time between images, the motion trajectory, and the scene itself. Examining this relationship allows the designer to predict, and potentially compensate for, the effects of lower quality inertial sensors by varying the image sampling rate.

As a result of this relationship, the image sample rate is increased by 2.5 times in order to compensate for the lower performance level of the consumer-grade IMU compared to the tactical-grade sensor. This resulted in a 2.5 Hz image collection rate, which was the upper limit of the recording hardware.

SYSTEM TESTS

The imaging and inertial fusion navigation algorithm is evaluated using both simulated and experimental ground profiles. The profiles are designed to provide a range of image types in order to exercise the feature tracking algorithm. The simulation and results are presented in the next section.

The data collection system consisted of a consumer-grade MEMS IMU and two digital cameras (see Figure 3). The IMU was a Crista consumer-grade MEMS unit which measured acceleration and angular rate at 100 Hz. The digital cameras were both Pixelink A-741 machine vision cameras which incorporated a global shutter feature and a Firewire interface. The lenses were wide-angle Pentax lenses with approximately 90 degrees field of view. The sensors were mounted on an aluminum plate and calibrated using procedures similar to those described in [22]. Images were captured at approximately 2.5 Hz. In addition, a Honeywell HG1700, tactical-grade inertial measurement unit was co-mounted on the platform in order to provide a one-to-one performance comparison between different grades of inertial sensors.

Simulation

The algorithm was tested using a Monte Carlo simulation

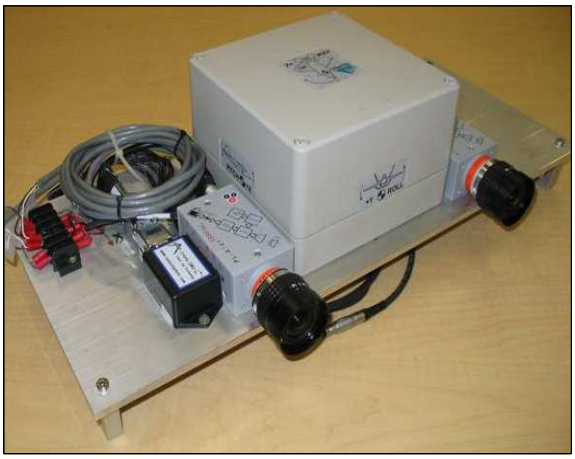

Figure 3: *Data collection system. The data collection system consisted of a consumer-grade MEMS IMU and monochrome digital cameras. A tactical-grade IMU was co-mounted on the platform in order to provide a performance comparison between different grades of inertial sensors.*

of a standard indoor profile. The profile consisted of a straight corridor, designed to be similar to the indoor experimental data collection.

An accurate simulation of the navigation environment requires simulating the performance of the sensors in response to a true motion trajectory. The trajectory was generated using ProfGen version 8.19 software package [11]. For each Monte Carlo navigation simulation run, the inertial sensor measurements are generated using the true trajectory and an inertial sensor error model.

Because of the inherent complexity of the optical environment, it is beyond the scope of this paper to generate simulated images. Instead, a simulated feature set was created by randomly distributing features along a corridor surrounding the true trajectory. The features are each given random descriptor vectors in order to exercise the feature tracking algorithm. While this optical simulation method is appropriate for testing the image and inertial fusion algorithm, the results are not directly comparable to the real system performance, because imaging issues such as lighting conditions, motion blur, and affine changes in the feature descriptor due to pose changes are not modeled.

The simulated corridor was 3 meters wide, 3 meters high, and approximately 300 meters long. Features were randomly generated on the walls, floor and ceiling of the corridor with an average spacing of 0.25 features per square meter. Each feature was given a random primary length and orientation, which, combined with the true pose of the sensor, resulted in accurately simulated scale and orientation parameters in feature space. After a 60-second stationary alignment, the sensor platform accelerated to 0.5 meters per second, maintained this velocity until the end of the corridor, then accelerated to a stop at the end. The platform remained stationary for 60 seconds after coming to a stop. This resulted in a 660-second image and inertial navigation profile. Simulated images are collected at 2 Hz.

A Monte Carlo simulation was conducted using inertial sensor models representing the H1700 tactical-grade IMU and the Crista consumer-grade IMU. Each simulation consisted of 60 runs, each with randomly generated inertial measurement errors due to random walks, sensor bias, and sensor scale-factor errors. In order to mitigate any potential effects due to the location of the features in the simulated environment, the feature locations and descriptors were randomly generated every 20 runs.

The position errors using the tactical-grade IMU are shown in Figures 4. As expected, the inertial and imaging measurement errors accumulate, resulting in position drift.

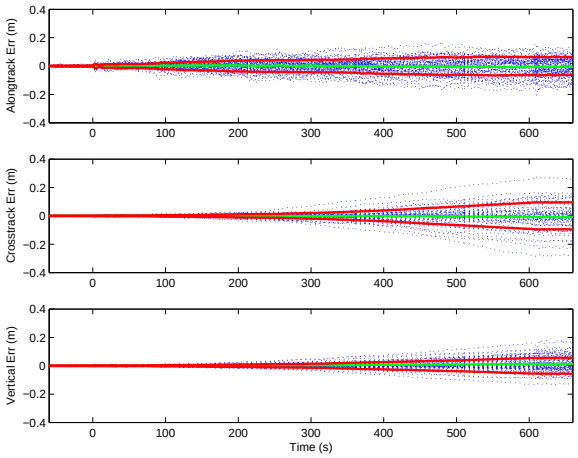

Figure 4: *Simulated 60-run Monte Carlo position error results for indoor profile with a tactical-grade inertial sensor and image aiding using landmarks of opportunity. The position error sample functions are indicated by blue dotted lines. The ensemble mean and standard deviation are indicated by the green and red solid lines, respectively.*

The position errors using the consumer-grade IMU are shown in Figures 5. In addition to proportionally larger errors in position, significant excursions in position are noted, which are the effects of increased attitude errors.

Root-sum-squared (RSS) errors are analyzed in order to provide a one-dimensional metric for a more direct comparison of the simulated system performance for different profiles. The RSS errors comparing the free-inertial and image-aided performance is shown in Figures 6-8. Over the 10-minute indoor profile, incorporating the image-aiding measurements improves the errors for both the consumer and tactical-grade sensors by many orders of magnitude.

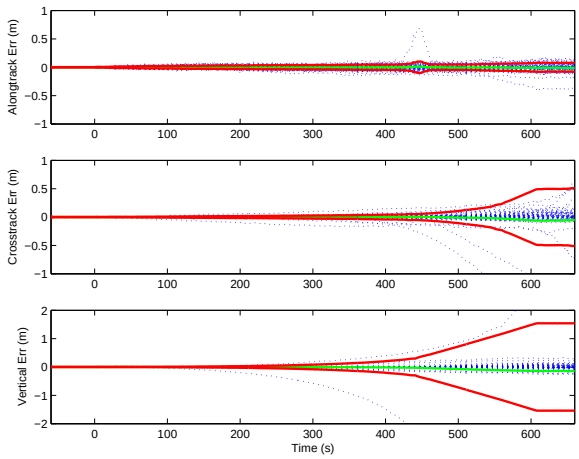

Figure 5: *Simulated 60-run Monte Carlo position error results for indoor profile with a consumer-grade inertial sensor and image aiding using landmarks of opportunity. The position error sample functions are indicated by blue dotted lines. The ensemble mean and standard deviation are indicated by the green and red solid lines, respectively.*

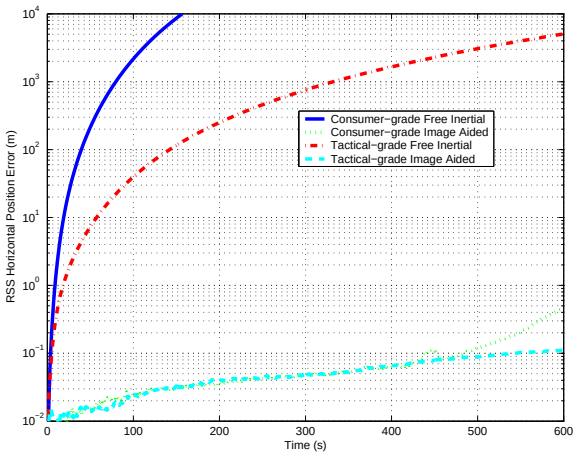

Figure 6: *Simulated 60-run Monte Carlo root-sum-squared (RSS) horizontal position error for indoor profile using both consumer-grade and tactical-grade inertial sensors. The results are shown for four cases: 1) consumer-grade free inertial, 2) consumer-grade opportunity landmark tracking, 3) tactical-grade free inertial, and 4) tactical-grade opportunity landmark tracking.*

In addition, the image-aided consumer-grade sensor nearly equals the position error performance of the image-aided tactical-grade sensor, until the consumer-grade sensor begins to show some attitude divergences after approximately 400 seconds.

In the next section, the experimental data collection profiles and results are presented.

Experiment

The algorithm is tested experimentally using two ground navigation profiles designed to examine the operation of the feature tracking system in a real-world environment. The profile consisted of a closed path in an indoor environment. The path began and ended at the same location and orientation in the Advanced Navigation Technology (ANT) Center laboratory, at the Air Force Institute of Technology. As in the previous profile, the data collection began with a 10-minute stationary alignment period. After the alignment period, the sensor was moved in a 10-minute loop around the hallways of the building. In contrast to the previous profile, the sensor was pointed primarily in the direction of travel. No prior knowledge was provided to the algorithm regarding the location of features or structure of the environment. A sample image from the indoor profile is shown in Figure 9.

The indoor profile presents the algorithm with different challenges from a feature tracking perspective. The indoor environment consists of repetitive, visually identical features (e.g., floor tiles, lights, etc.), which can easily cause confusion for the feature tracking algorithm. In addition, reflections from windows and other shiny surfaces might not be interpreted properly by the filter and could potentially result in navigation errors. Finally, the lower light intensity levels and large areas with poor contrast (e.g., smooth, featureless walls) presents a relatively stark feature space. The indoor profile is performed twice for both the tactical and navigation-grade sensors.

The filters' estimates of the trajectories are overlayed on a floor plan of the building in Figures 10 and 11 for the tactical and consumer-grade inertial sensors, respectively. In each figure, a comparison is made between the fused image-aided inertial trajectory estimate, the image-aided inertial trajectory with stochastic constraints disabled, and a free inertial trajectory. For both tactical and consumer-grade sensors, the estimated trajectory generally corresponds to the building's hallways, with excursions of less than 3 meters. In addition, the results of the free-inertial trajectories show the inherent lack of accuracy of the inertial sensor. With stochastic constraints purposely disabled, the trajectory estimates show relatively large trajectory errors due to false correspondence matches. This illustrates the catastrophic effects of incorporating false updates into an Extended Kalman Filter with inertial feedback and demonstrates the inherent strength of applying robust correspondence methods, and in particular stochastic constraints.

The filter's estimated trajectory for the image-aided consumer-grade sensor (run two) is examined in more detail in Figure 14, where the estimated location of landmarks

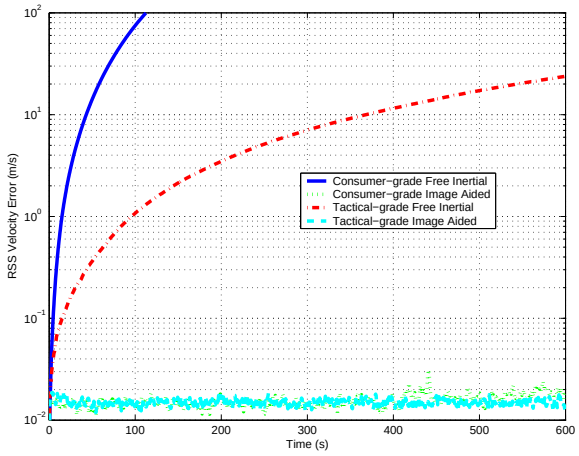

Figure 7: *Simulated 60-run Monte Carlo root-sum-squared (RSS) velocity error for indoor profile using both consumer-grade and tactical-grade inertial sensors. The results are shown for four cases: 1) consumer-grade free inertial, 2) consumer-grade opportunity landmark tracking, 3) tactical-grade free inertial, and 4) tactical-grade opportunity landmark tracking.*

used for tracking are highlighted. Note the landmarks correspond to the building walls, ceilings, and floors. More detail of the start/stop area is shown in Figure 13. A comparison of all image-aided inertial navigation results for both the tactical and consumer-grade sensors is shown in Figure 12. The difference in the estimated start and stop locations shows the accumulated errors in the filter over the path. Over the 10-minute profile, the path closure errors are less than 5 *m* in the horizontal plane and less than 5 *m* in the vertical for all sensors. Again, this is a significant improvement over the free-inertial performance.

In each case, incorporation of image updates into the navigation filter improves the position error by several orders of magnitude over the respective inertial-only solutions. In addition, the integrated consumer-grade inertial solution demonstrates nearly equivalent performance to the integrated tactical-grade inertial solution.

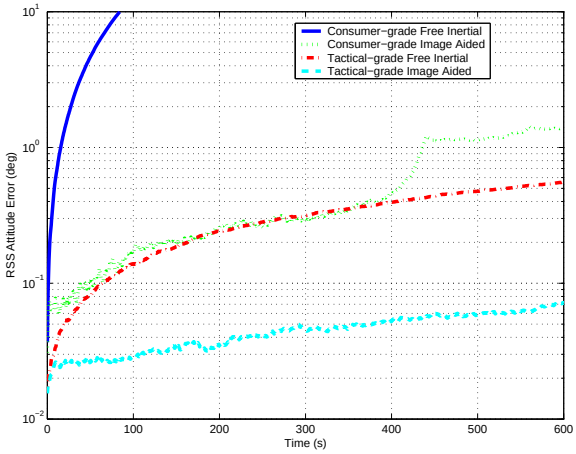

Figure 8: *Simulated 60-run Monte Carlo root-sum-squared (RSS) attitude error for indoor profile using both consumer-grade and tactical-grade inertial sensors. The results are shown for four cases: 1) consumer-grade free inertial, 2) consumer-grade opportunity landmark tracking, 3) tactical-grade free inertial, and 4) tactical-grade opportunity landmark tracking.*

Figure 9: *Sample image from indoor data collection. The indoor data collection presents the filter with man-made features in an office environment. The crosses and ellipses indicate the locations and uncertainty of currently tracked landmarks.*

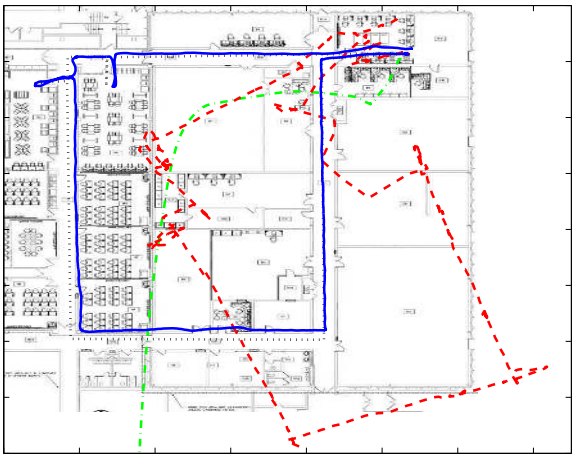

Figure 10: *Estimated path from indoor data collection (run two) using tactical-grade inertial sensor. The filter's estimate of the path (indicated by the solid line) agrees well with the known path (indicated by the dotted line). The inertial-only best estimate of trajectory (indicated by the dash-dotted line) and image-aided inertial with stochastic constraints disabled (indicated by the dashed line) show large errors in position and heading. The inertial-only solution exceeds the scale of the image after 156 seconds.*

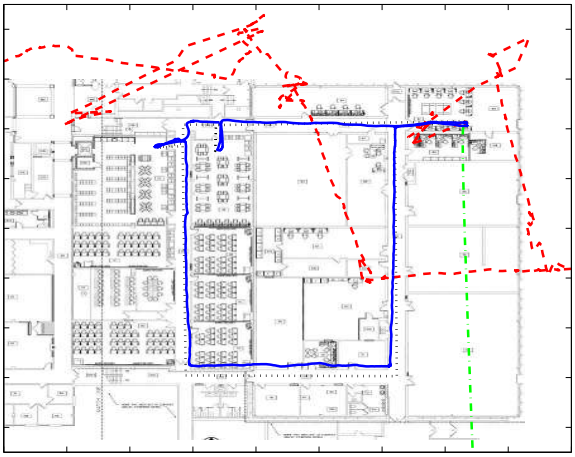

Figure 11: *Estimated path from indoor data collection (run two) using consumer-grade inertial sensor. The filter's estimate of the path (indicated by the solid line) agrees well with the known path (indicated by the dotted line). The inertial-only best estimate of trajectory (indicated by the dash-dotted line) and image-aided inertial with stochastic constraints disabled (indicated by the dashed line) show large errors in position and heading. The inertial-only solution exceeds the scale of the image after 11 seconds.*

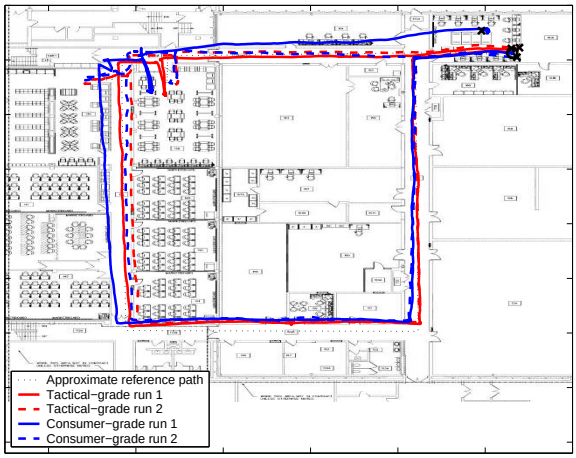

Figure 12: *Performance comparison for image-aided tactical and consumer-grade inertial sensors for indoor profile runs one and two. The common start and stop location for both runs is indicated by the "o" symbol. The estimated stop location for each run is indicated by an "x" symbol.*

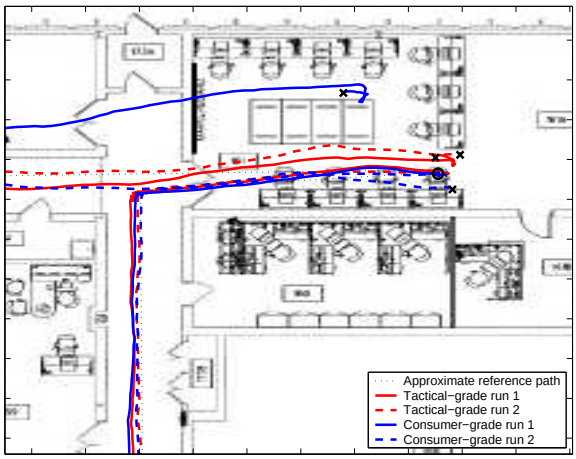

Figure 13: *Enhanced detail of the start/stop area illustrating the estimated trajectory and feature locations for both the image-aided tactical and consumer-grade inertial sensors for indoor profile runs one and two. The difference between the estimated start and stop location illustrates the accumulated position error.*

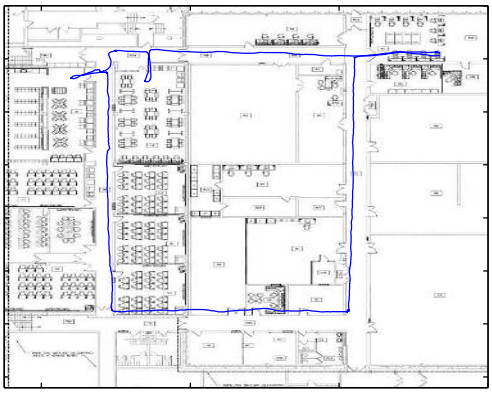

a) Entire path estimate

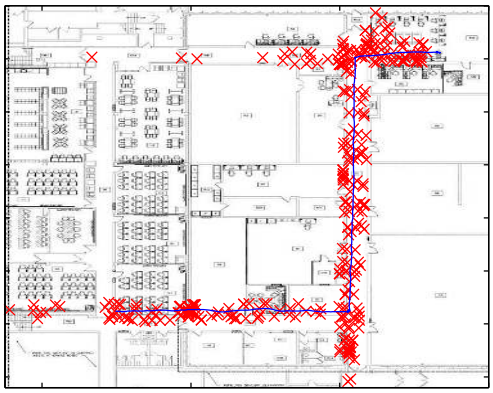

b) First half of path with tracked feature locations

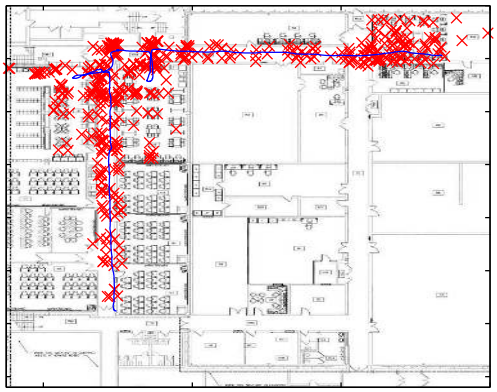

c) Second half of path with tracked feature locations

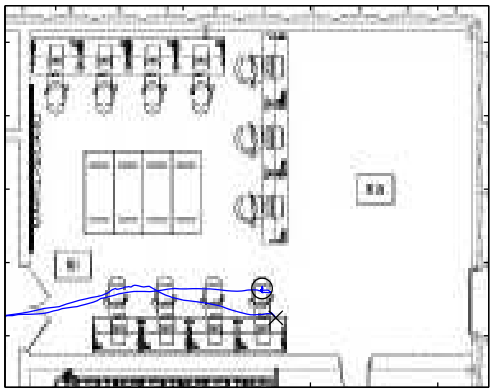

d) Start/stop area detail

Figure 14: *Estimated path and feature locations from indoor data collection (run two) for consumer-grade inertial sensor. Pane (a) shows the entire path estimate. Pane (b) shows the first half of the path along with the estimated location of the features (indicated by "x" symbols). Pane (c) shows the last half of the path and estimated feature locations. Pane (d) provides detail of the start/stop area.*

CONCLUSIONS

In this paper, an algorithm is presented which integrates low-cost inertial and image sensors to provide an enhanced navigation solution. The integration is accomplished using a fusion technique designed to tightly-couple the respective sensors using a statistically-rigorous feature transformation algorithm.

The integrated system was tested using a combination of Monte Carlo simulation and experimental data collections. The simulation predicted a significant improvement by fusing image and inertial measurements for both the consumer and tactical-grade inertial sensors. In addition, the simulation revealed small differences in attitude-error stability, which negatively influenced the long-term stability of the integrated consumer-grade sensor over the integrated tactical-grade sensor.

The experiment demonstrated multiple orders-of-magnitude improvement between image-aided and unaided inertial position solutions. Over the 10-minute, unconstrained, indoor-profile, both integrated sensors exhibited closed-path navigation errors of less than 5 meters, which is a significant improvement over the respective unaided systems.

In summary, this research develops a series of techniques to provide autonomous, passive navigation by incorporating image and inertial measurements. The method demonstrates navigation-quality performance using only low-cost sensors and passive updates.

DISCLAIMER

The views expressed in this article are those of the author and do not reflect the official policy or position of the United States Air Force, Department of Defense, or the U.S Government.

References

[1] H. Adams, S. Singh, and D. Strelow. An Empirical Comparison of Methods for Image-based Motion Estimation. In *Proceedings of the 2002 IEEE/RSJ Intl. Conference on Intelligent Robots and Systems*, volume 1, pp. 123–128, September 2002.

[2] A. Brown and Y. Lu. Performance Test Results of an Integrated GPS/MEMS Inertial Navigation Package. In *Proceedings of ION GNSS 2004*, pp. 825–832, September 2004.

[3] R. G. Brown and P. Y. Hwang. *Introduction to Random Signals and Applied Kalman Filtering*. John Wiley and Sons, Inc., New York, NY, 1992.

[4] E. Hagen and E. Heyerdahl. Navigation by Optical Flow. In *Proceeding of the 11th IAPR International Conference on Pattern Recognition*, volume 1, pp. 700–703, 1992.

[5] S. Hrabar and G. S. Sukhatme. A Comparison of Two Camera Configurations for Optic-Flow Based Navigation of a UAV Through Urban Canyons. In *Proceedings of the 2004 IEEE/RSJ International Conference on Intelligent Robots and Systems*, volume 3, pp. 2673–2680, September 2004.

[6] C. Liebe. Star trackers for attitude determination. *Aerospace and Electronic Systems Magazine, IEEE*, 10(6):10–16, June 1995.

[7] D. G. Lowe. Object Recognition from Local Scale-Invariant Features. In *Proc. of the International Conference on Computer Vision*, volume 2, pp. 1150–1157, September 1999. Corfu, Greece.

[8] Y. Ma, S. Soatto, J. Kosecka, and S. S. Sastry. *An Invitation to 3-D Vision*. Springer-Verlag, Inc., New York, New York, 2004.

[9] P. S. Maybeck. *Stochastic Models Estimation and Control, Vol I*. Academic Press, Inc., Orlando, Florida 32887, 1979.

[10] P. S. Maybeck. *Stochastic Models Estimation and Control, Vol II*. Academic Press, Inc., Orlando, Florida 32887, 1979.

[11] S. Musick. Profgen: PC Software for Trajectory Generation. Software Package v8.19, Air Force Research Laboratory, Wright-Patterson Air Force Base, Ohio, January 2004.

[12] C. F. Olson, L. H. Matthies, M. Schoppers, and M. W. Maimone. Robust Stereo Ego-motion for Long Distance Navigation. In *Proceedings of the IEEE Conference on Advanced Robotics*, volume 2, pp. 453–458, June 2000.

[13] M. Pachter and A. Porter. Bearings-only Measurements for INS Aiding: The Three-Dimensional Case. In *Proceedings of the 2003 AIAA Guidance, Navigation and Control Conference*, 2003. AIAA paper number 2003-5354.

[14] M. Pachter and A. Porter. INS Aiding by Tracking an Unknown Ground Object - Theory. In *Proceedings of the American Control Conference*, volume 2, pp. 1260–1265, 2003.

[15] P. Pissavin, J. Krebs, P. LeLong, P. Vidal, and R. Navoni. Improved Star Tracker for ODIN Satellite. In *Proceedings of ESA International Conference on Spacecraft Guidance, Navigation and Control Systems*, pp. 611–616, November 1997.

[16] D. Purll, N. Gradmann, and M. Bollner. The ROSAT Star Tracker: Flight Experience. *ESA, Spacecraft Guidance, Navigation and Control Systems*, N92-2443215-18:551–556, 1991.

[17] J. F. Raquet and M. Giebner. Navigation Using Optical Measurements of Objects at Unknown Locations. In *Proceedings of the 59th Annual Meeting of the Institute of Navigation*, pp. 282–290, June 2003.

[18] J. F. Raquet, M. Giebner, and M. J. Veth. Navigation Using Optical Measurements of Objects at Unknown Locations. ?, December 2004.

[19] D. Strelow and S. Singh. Optimal Motion Estimation from Visual and Inertial Measurements. In *Proceedings of the Workshop on Applications of Computer Vision*, December 2002.

[20] D. W. Strelow. *Motion Estimation from Image and Inertial Measurements*. PhD thesis, School of Computer Science, Carnegie Mellon University, Pittsburgh, PA 15213, November 2004.

[21] D. Titterton and J. Weston. *Strapdown Inertial Navigation Technology*. Peter Peregrinus Ltd., Lavenham, United Kingdom, 1997.

[22] M. J. Veth and J. F. Raquet. Alignment and Calibration of Optical and Inertial Sensors Using Stellar Observations. In *Proceedings of ION GNSS 2005*, pp. 2494–2503, September 2005.

[23] M. J. Veth and J. F. Raquet. Two-Dimensional Stochastic Projections for Tight Integration of Optical and Inertial Sensors for Navigation. In *National Technical Meeting Proceedings of the Institute of Navigation*, pp. 587–596, 2006.

[24] M. J. Veth, J. F. Raquet, and M. Pachter. Stochastic Constraints for Robust Image Correspondence Search. *IEEE Transactions on Aerospace Electronic Systems*, Publication forthcoming.